# Capillary saturation and desaturation

R. Hilfer
ICP, University of Stuttgart, 70569 Stuttgart, Germany

R. T. Armstrong
School of Petroleum Engineering, University of New South Wales, NSW, 2052 Sydney, Australia

S. Berg, A. Georgiadis, and H. Ott
Shell Global Solutions International B.V., 2288 GS Rijswijk, Netherlands

originally published in: Physical Review E
originally submitted: June 3rd, 2015; published: December 23rd, 2015

DOI: 10.1103/PhysRevE.92.063023; PACS number(s): 47.56.+r,81.05.Rm

**Abstract**

Capillary desaturation experiments produce disconnected (trapped) ganglia of mesoscopic sizes intermediate between pore size and system size. Experimental evidence for interactions between these mesoscale clusters during desaturation is analyzed and discussed within the established microscopic and macroscopic laws of Newton, Young-Laplace and Darcy. A theoretical expression for capillary number correlations is introduced that seems to have remained unnoticed. It expresses capillary desaturation curves in terms of stationary capillary pressures and relative permeabilities. The theoretical expression shows that the plateau saturation in capillary desaturation curves may in general differ from the residual nonwetting saturation defined through the saturation limit of the main hysteresis loop. Hysteresis effects as well as the difference between wetting and nonwetting fluids are introduced into the analysis of capillary desaturation experiments. The article examines experiments with different desaturation protocols and discusses the existence of a mesoscopic length scale intermediate between pore scale and sample scale. The theoretical expression is derived entirely within the existing traditional theory of two-phase flow in porous media and compared to a recent experiment.

CONTENTS

*[page 1, §1]*

# I. Introduction

*[1.1.1.1]* A capillary desaturation experiment measures the volume of fluid flowing out from a porous medium as a result of injecting a second fluid (immiscible with the first) at varying injection rates. *[1.1.1.2]* Displacement of a nonwetting fluid by a wetting fluid is of great importance for hydrocarbon production processes [1–3].

*[1.1.2.1]* Most capillary desaturation experiments are carried out in "discontinuous mode". *[1.1.2.2]* A discontinuous mode desaturation typically starts from a sample filled with nonwetting fluid and increases the injection rate of the wetting fluid in steps, i.e. with a step function protocol in time. *[1.1.2.3]* It is called "discontinuous mode" because the configuration of the residual fluid is discontinuous in the sense of not connected from inlet to outlet. *[1.1.2.4]* On the other hand in a "continuous mode" desaturation one starts always from a continuous initial configuration in which the resident fluid is hydraulically connected to the inlet and outlet. *[1.1.2.5]* Rather than increasing the injection rate sequentially the sample is emptied, refilled and then injected at with a new (increased) rate. *[1.1.2.6]* Experiments in continuous mode are more laborious and expensive than discontinuous mode experiments. *[1.1.2.7]* Many experiments report a constant plateau saturation of the remaining resident fluid at small injection rates followed by a gradual decrease at higher injection rates, as seen for example in Figures 3-17, 3-18, 3-19, pp 70–73 of [3].

*[1.1.3.1]* Dimensionless (or scaling) groups are algebraic combinations of the constitutive parameters from the mathematical model. *[1.1.3.2]* Examples, such as the Reynolds or Peclet number, arise in many fields of physical science. *[1.1.3.3]* In capillary desaturation experiments the results are commonly given in terms of the capillary number, which quantifies the ratio of viscous to capillary forces.

*[1.2.1.1]* Given the correlation between displacement efficiency and capillary number during water flooding, it is believed that mobilization of residual nonwetting fluid depends predominantly on the competition between viscous and capillary forces [4]. *[1.2.1.2]* Less importance is usually attributed to other factors such as initial fluid configuration, desaturation protocol, mesoscopic cluster interactions and/or the nature of the displacement processes (drainage vs. imbibition) during the experiment. *[1.2.1.3]* One of our motivations for this work is to advance the study of these additional factors influencing capillary desaturation experiments. *[1.2.1.4]* Recent experiments [5–7] have called for studies of the process dependence. *[1.2.1.5]* In this work we take up such studies by analyzing these desaturation experiments. *[1.2.1.6]* As a result we propose to perform not only desaturation expriments, but also saturation experiments in which the nonwetting saturation increases rather than decreases during stationary wetting fluid flow. *[1.2.1.7]* Mobilization and trapping, coalescence and breakup of nonwetting fluid then determines the increase of nonwetting saturation in the same way as in desaturation experiments from the competition between viscous and capillary forces.

*[1.2.2.1]* Recovery of residual oil during waterflooding depends upon how small the capillary forces become relative to viscous forces. *[1.2.2.2]* Accordingly, the results of capillary desaturation experiments are generally presented as functions of various capillary numbers instead of injection rates, because capillary numbers are supposed to reflect the force balance. *[1.2.2.3]* A capillary number is a dimensionless group

$$\mathrm{Ca} = \frac{\text{(viscous forces)}}{\text{(capillary forces)}} \tag{1}$$

that quantifies the ratio of viscous to capillary forces. *[1.2.2.4]* Ideally, the condition $\mathrm{Ca} \approx 1$ marks the transition from capillary dominated to viscous dominated flow. *[1.2.2.5]* Numerous definitions of capillary numbers, however, do not fulfill this expectation as shown in [8–10].

*[page 2, §1]* *[2.1.1.1]* Herein, we present a new formulation for the force balance between viscous and capillary forces of macroscale two-phase flow that has previously been overlooked. *[2.1.1.2]* This new finding is based on introducing the force balance $F$ quantitatively into eq. (1) by writing

$$\frac{\text{(viscous pressure drop)}}{\text{(capillary pressure)}} = F(S, v, L) \tag{2}$$

and investigating its dependence on saturation $S$, velocity $v$ and system size $L$. *[2.1.1.3]* This simple exercise has, to the best of our knowledge, never been done and turns up a surprising result that is applicable to capillary desaturation. *[2.1.1.4]* The main new result of our investigation is eq. (27) below, which expresses the force balance $F(S, v, L) = f(S, \mathrm{Ca})$ quantitatively as a function of saturation and the macroscopic capillary number $\mathrm{Ca}$ introduced in [9]. *[2.1.1.5]* Setting $F = F_0$ to some fixed value $F_0$ generates capillary number correlations $S = S_{F_0}(\mathrm{Ca})$ that seem to be new. *[2.1.1.6]* Capillary number correlations appear in capillary desaturation experiments, and were heretofore not predictable within the traditional theoretical framework. *[2.1.1.7]* Our new findings provide a means to develop theoretical capillary desaturation curves that compare well to experimental results.

*[2.1.2.1]* The article is organized as follows: *[2.1.2.2]* Section II formulates the problem as a problem of length scales. *[2.1.2.3]* Mobilization and recovery of residual oil produces disconnected nonwetting clusters whose average extension is determined by a balance of viscous and capillary forces. *[2.1.2.4]* Section II also formulates six specific objectives that have been addressed and achieved. *[2.1.2.5]* Section III introduces notation and, more importantly, formulates scale separation between microscopic pore scale and macroscopic laboratory scale. *[2.1.2.6]* The mathematically precise formulation of scale separation was crucial for all of our subsequent analysis.

*[2.1.3.1]* Section IV gives a brief analysis of force balance and capillary number on the pore scale. *[2.1.3.2]* Section V discusses the force balance and capillary number on the sample scale uncovering eq. (27) as the main new result. *[2.1.3.3]*

Section VI relates the main new result to a variety of alternative definitions for capillary number and visco-capillary force balance. *[2.1.3.4]* This discussion is crucial for the subsequent application of eq. (27) to experiment in Section VII. *[2.1.3.5]* Equally important is the experimental fact that capillary desaturation experiments depend critically on the desaturation protocol. *[2.1.3.6]* Accordingly, Section VII defines and distinguishes various experimental protocols in these experiments. *[2.1.3.7]* It then applies eq. (27) in two ways: Firstly, to discuss and analyse the recent experiments of [5]. *[2.1.3.8]* The result is presented in Figure 3. *[2.1.3.9]* Secondly, to propose a new experiment (with the protocol specified in eq. (56)) and predict its outcome in Figure 4. *[2.1.3.10]* Figures 3 and 4 are the main results demonstrating the fruitful application of eq. (27) to existing experiments as well as its predictive power for new experiments.

*[2.1.4.1]* Section VIII places the main results of eq. (27), Fig. 3 and Fig. 4 in a broader context. *[2.1.4.2]* It discusses protocol dependence, plateau saturation, cooperative dynamics and inertial effects. *[2.1.4.3]* This discussion achieves the objectives formulated in Section II. *[2.1.4.4]* The article concludes with a summary of results. *[2.1.4.5]* The motivating question of length scales can, at present, not be answered with yes or no. *[2.2.0.6]* However, investigating this question has uncovered new facts related to the importance of nonpercolating fluid parts for residuals, capillary desaturation and macroscopic two phase immiscible displacement.

## II. Problem and Objectives

*[2.2.1.1]* The problem to be discussed in this article is the question of whether or not there exists a mesoscopic length scale with new constitutive laws intermediate between the microscopic pore scale $\ell$ and the macroscopic sample size $L$. *[2.2.1.2]* Recent capillary desaturation experiments in [5, 11] seem to hint towards the possible existence of a mesoscopic length scale. *[2.2.1.3]* Existing theories do not explain or predict capillary desaturation curves or spatiotemporal changes of nonpercolating residual saturations. *[2.2.1.4]* Direct upscaling from pore to sample scale may be difficult or impossible, because mesoscopic nonpercolating clusters and their interaction become important [12–14].

*[2.2.2.1]* The theoretical importance of nonpercolating trapped clusters (ganglia) on macroscopic scales (Darcy scale and larger) was emphasized already in [15]. *[2.2.2.2]* It was thoroughly analyzed in [16] and [17]. *[2.2.2.3]* The results of this analysis led to the proposal of a generalized macroscopic theory [18] predicting hysteresis [19], recovering the traditional theory [20] and highlighting the role of interfacial areas in [21]. *[2.2.2.4]* Experimental evidence for the possible importance of a mesoscopic scale seems to have been found in recent experimental advances allowing *in situ* monitoring of immiscible displacement processes using fast X-ray computed microtomography [5]. *[2.2.2.5]* Theoretical evidence for the importance of clusters on macroscopic scales was found in [22] for immiscible fluids in hydrostatic equilibrium, in [23] for raising and/or rotating closed columns, in [24] for Buckley-Leverett shocks, in [25] for McWhorter-Sunada flows and capillarity driven horizontal redistribution (Philip-problem), in [26] for saturation overshoot, and in [27] for multistep outflow experiments. *[2.2.2.6]* Recent drainage and imbibition experiments with pore scale imaging performed by [11] confirm that the dynamics is nonlocal and that capillary action at menisci is percolating over some mesoscopic distance. *[2.2.2.7]* These experimental observations and theoretical advances all seem to hint towards a mesoscopic cluster scale, that might be defined via the nonpercolating clusters and their interaction with each other.

*[2.2.3.1]* The main objectives of this paper are:

(i) to study the process dependence of capillary desaturation curves and the dependence on the desaturation protocol,
(ii) to introduce new capillary saturation curves for oil injection based on traditional two-phase flow theory,
(iii) to propose new capillary saturation experiments with oil injection instead of water injection,
(iv) to introduce a new relation between capillary desaturation curves and the product of relative permeabilities with normalized capillary pressure functions that seems to have remained unnoticed so far,
(v) to show that the plateau saturation in capillary desaturation curves is not given as the residual oil saturation $S_{\mathbb{O}\,\mathrm{r}}$ (defined in eq. (25b) below), but can be either $1 - S_{\mathbb{W}\,\mathrm{i}}$ (where the irreducible water saturation $S_{\mathbb{W}\,\mathrm{i}}$ is defined in eq. (25a) below) or any saturation below $1 - S_{\mathrm{z}}$ where $S_{\mathrm{z}}$ is defined as the zero $P_{\mathrm{c}}^{\,\mathrm{imb}}(S_{\mathrm{z}}) = 0$ on the capillary pressure curve for secondary imbibition, and
(vi) to quantify the large variation of breakpoints in capillary desaturation curves within the traditional two-phase flow theory.

*[page 3, §1]*

## III. Preliminaries

### A. Notation

*[3.1.1.1]* Time is denoted as $t \in \mathbb{R}$ and position as $\mathbf{x} \in \mathbb{R}^3$. *[3.1.1.2]* The geometry of the porous medium and its fluid content is represented mathematically by several closed subsets of $\mathbb{R}^3$. *[3.1.1.3]* These are

$$\mathbb{R}^3 \supset \mathbb{S} := \text{sample core} \tag{3a}$$
$$\mathbb{S} \supset \mathbb{P} := \text{pore space} \tag{3b}$$
$$\mathbb{S} \supset \mathbb{S} \setminus \mathbb{P} = \mathbb{M} := \text{matrix space} \tag{3c}$$
$$\mathbb{P} \supset \mathbb{W}(t) := \text{wetting fluid at time } t \tag{3d}$$
$$\mathbb{P} \supset \mathbb{P} \setminus \mathbb{W}(t) = \mathbb{O}(t) := \text{non-wetting fluid at time } t \tag{3e}$$

where $\mathbb{W}$ stands for water (wetting) and $\mathbb{O}$ for oil (non-wetting). *[3.1.1.4]* The wetting and nonwetting fluid are assumed to be immiscible. *[3.1.1.5]* The Euclidean position space $\mathbb{R}^3$ carries the usual topology, metric structure and Lebesgue measure $\mathrm{d}^3x$. *[3.1.1.6]* The volume of a subset $\mathbb{G} \subset \mathbb{R}^3$ is defined and denoted as

$$|\mathbb{G}| := \int_{\mathbb{R}^3} \chi_{\mathbb{G}}(\mathbf{x})\, \mathrm{d}^3\mathbf{x} = \int_{\mathbb{G}} \mathrm{d}^3\mathbf{x} \tag{4}$$

where

$$\chi_{\mathbb{G}}(x) := \begin{cases} 1 & \text{for } x \in \mathbb{G} \\ 0 & \text{for } x \notin \mathbb{G} \end{cases} \tag{5}$$

is the characteristic (or indicator) function of a set $\mathbb{G}$. *[3.1.1.7]* The interior $\mathrm{in}(\mathbb{G})$ of a set $\mathbb{G}$ is the union of all open sets contained in the set $\mathbb{G}$. *[3.1.1.8]* It is assumed that

$$\mathbb{S} = \mathbb{P} \cup \mathbb{M}, \qquad \mathrm{in}(\mathbb{P}) \cap \mathrm{in}(\mathbb{M}) = \emptyset \tag{6}$$

holds and the volume fraction

$$\phi = \frac{|\mathbb{P}|}{|\mathbb{S}|} = 1 - \frac{|\mathbb{M}|}{|\mathbb{S}|} \tag{7}$$

is called porosity. *[3.1.1.9]* The *surface*, or *boundary*, of a set $\mathbb{G}$ is denoted as $\partial\mathbb{G}$. *[3.1.1.10]* All boundaries are assumed to be sufficiently smooth. *[3.1.1.11]* The set $\mathbb{P} \cap \mathbb{M} = \partial\mathbb{P} \setminus \partial\mathbb{S} = \partial\mathbb{M} \setminus \partial\mathbb{S}$ is the rigid internal boundary between $\mathbb{P}$ and $\mathbb{M}$.

*[3.1.2.1]* It will be assumed throughout, that the sets $\mathbb{P}$ and $\mathbb{M}$ are pathconnected. *[3.1.2.2]* A set is called pathconnected if any two of its points can be connected by a path contained inside the set. *[3.1.2.3]* This excludes isolated disconnected pores and grains [28, Problem 6.(a), p. 120]. *[3.1.2.4]* Moreover, it will be assumed that $\partial\mathbb{P} \cap \partial\mathbb{S} \neq \emptyset$ and $\partial\mathbb{M} \cap \partial\mathbb{S} \neq \emptyset$. *[3.1.2.5]* Analogous to eq. (6) also the fluid regions are disjoint except for their boundary, i.e.

$$\mathbb{P} = \mathbb{W}(t) \cup \mathbb{O}(t), \qquad \mathrm{in}(\mathbb{W}(t)) \cap \mathrm{in}(\mathbb{O}(t)) = \emptyset \tag{8}$$

holds for all $t$. *[3.1.2.6]* Their volume fractions

$$S_{\mathbb{W}}(t) = \frac{|\mathbb{W}(t)|}{|\mathbb{P}|} = \frac{|\mathbb{P} \setminus \mathbb{O}(t)|}{|\mathbb{P}|} = 1 - S_{\mathbb{O}}(t) \tag{9}$$

are called saturations. *[3.1.2.7]* The volumetric injection rates of the two immiscible and incompressible fluids are denoted for $i = \mathbb{W}, \mathbb{O}$ as

$$Q_i = \text{volumetric injection rate of fluid } i \tag{10}$$

and have units of $\mathrm{ms}^{-1}$. *[3.2.0.8]* Matrix rigidity implies

$$Q(t) = Q_{\mathbb{W}}(t) + Q_{\mathbb{O}}(t) \tag{11}$$

where $Q(t)$ is the total volumetric flux.

## B. Scale separation

*[3.2.1.1]* Porous media physics requires to distinguish the microscopic pore scale $\ell$ from the macroscopic sample scale $L$. *[3.2.1.2]* The two scales are related by coarse graining or, mathematically, by a scaling limit as emphasized in [29, 30]. *[3.2.1.3]* The two scales will be distinguished by a tilde $\widetilde{\ }$ for microscopic pore scale quantities when necessary. *[3.2.1.4]* Thus $\widetilde{\mathbf{x}} \in \widetilde{\mathbb{R}}^3$ represents a position in the pore scale description, while $\mathbf{x} \in \mathbb{R}^3$ refers to a macroscale position. *[3.2.1.5]* The relation between $\widetilde{\mathbb{R}}^3$ and $\mathbb{R}^3$ may be symbolically written as $\mathbb{R}^3 \sim (\widetilde{\mathbb{R}}^3)^{\widetilde{\mathbb{R}}^3}$. *[3.2.1.6]* This expression symbolizes the formal relation

$$\widetilde{\mathbf{x}} = \varepsilon\mathbf{x} = \frac{\ell}{L}\mathbf{x}, \qquad \widetilde{\mathbf{x}} \in \widetilde{\mathbb{R}}^3,\ \mathbf{x} \in \mathbb{R}^3 \tag{12}$$

in the scaling limit $\varepsilon \to 0$. *[3.2.1.7]* To illustrate its meaning, consider the microscopic saturations

$$\widetilde{S_{\mathbb{W}}}(\widetilde{\mathbf{x}}, t) = \chi_{\mathbb{W}(t)}(\widetilde{\mathbf{x}}), \qquad \widetilde{\mathbf{x}} \in \widetilde{\mathbb{R}}^3 \tag{13a}$$

$$\widetilde{S_{\mathbb{O}}}(\widetilde{\mathbf{x}}, t) = \chi_{\mathbb{O}(t)}(\widetilde{\mathbf{x}}), \qquad \widetilde{\mathbf{x}} \in \widetilde{\mathbb{R}}^3 \tag{13b}$$

that are trivially defined in terms of characteristic functions. *[3.2.1.8]* Let

$$\varepsilon\mathbb{G} = \{\varepsilon\mathbf{x} : \mathbf{x} \in \mathbb{G}\}. \tag{14}$$

*[3.2.1.9]* The macroscopic saturations are to be understood formally as the scaling limit

$$S_{\mathbb{W}}(\mathbf{x}, t) = \lim_{\varepsilon\to 0} \frac{1}{|\varepsilon\mathbb{G}|} \int_{\mathbb{G}} \chi_{\mathbb{W}(t)}(\mathbf{x} + \varepsilon\mathbf{y})\, \mathrm{d}^3\mathbf{y}, \tag{15a}$$

$$S_{\mathbb{O}}(\mathbf{x}, t) = \lim_{\varepsilon\to 0} \frac{1}{|\varepsilon\mathbb{G}|} \int_{\mathbb{G}} \chi_{\mathbb{O}(t)}(\mathbf{x} + \varepsilon\mathbf{y})\, \mathrm{d}^3\mathbf{y}, \tag{15b}$$

where $\mathbf{x} \in \mathbb{S} \subset \mathbb{R}^3$ whenever this limit exists and is independent of $\mathbb{G}$. *[3.2.1.10]* Note that eq. (15) is formal, because the integrand is understood as a function of $\widetilde{\mathbf{y}} = \varepsilon\mathbf{y} \in \widetilde{\mathbb{R}}^3$. *[3.2.1.11]* For more mathematical rigour on homogenization see e.g. [31]. *[3.2.1.12]* Existence of the scaling limit is tantamount to the existence of an intermediate "representative elementary volume" $\mathbb{G}$ large compared to $\ell$ and small compared to $L$.

## IV. Microscopic pore scale $\ell$

*[3.2.2.1]* Consider stationary flow of a fluid inside the pore space $\mathbb{P}$. *[3.2.2.2]* On the pore scale the viscous forces are given quantitatively by Newton's law of internal friction

$$\begin{aligned}(\text{viscous pressure gradient}) &= \mu|\widetilde{\nabla}\widetilde{\mathbf{v}}| \\ &\approx \mu\frac{|\widetilde{\mathbf{v}}(\widetilde{\mathbf{x}}) - \widetilde{\mathbf{v}}(\widetilde{\mathbf{x}}_{\mathrm{wall}})|}{|\widetilde{\mathbf{x}} - \widetilde{\mathbf{x}}_{\mathrm{wall}}|}\end{aligned} \tag{16}$$

where $\mu$ is the fluid viscosity, $\widetilde{\nabla}\widetilde{\mathbf{v}}$ is the phase velocity gradient [*], and $\widetilde{\mathbf{v}}(\widetilde{\mathbf{x}}, t) = \widetilde{\mathbf{v}}(\widetilde{\mathbf{x}})$ is the phase velocity for stationary flow. *[page 4, §0]* *[4.1.0.1]* The capillary forces are quantified by the Young Laplace law as

$$(\text{capillary pressure}) = \sigma_{\mathbb{W}\mathbb{O}}\kappa \tag{17}$$

where $\sigma_{\mathbb{W}\mathbb{O}}$ is the interfacial tension and $\kappa$ the interfacial mean curvature in thermodynamic equilibrium between the two phases. *[4.1.0.2]* Using the same scale in both laws

$$|\widetilde{\mathbf{x}} - \widetilde{\mathbf{x}}_{\mathrm{wall}}| \approx \kappa^{-1} \approx \ell = (\text{pore diameter}), \tag{18a}$$

[*] In general $\widetilde{\nabla}\widetilde{\mathbf{v}}_i$ is a tensor of rank 2 and $\mu$ is a tensor of rank 4 yielding the fluid stress tensor of rank 2.

approximating $\widetilde{\mathbf{v}}(\widetilde{\mathbf{x}})$ by its spatial average $\widetilde{\mathbf{v}}$ as

$$\widetilde{\mathbf{v}}_i(\widetilde{\mathbf{x}}) \approx \widetilde{\mathbf{v}}_i = \frac{1}{|\mathbb{P}\cap\mathbb{S}|}\int_{\mathbb{S}} \chi_{\mathbb{P}}(\widetilde{\mathbf{y}})\widetilde{\mathbf{v}}_i(\widetilde{\mathbf{y}})\,\mathrm{d}^3\widetilde{\mathbf{y}} \tag{18b}$$

and using

$$\widetilde{\mathbf{v}}_i(\widetilde{\mathbf{x}}_{\mathrm{wall}}) = 0 \tag{18c}$$

for both phases $i = \mathbb{W}, \mathbb{O}$ one arrives at the microscopic capillary number

$$\widetilde{\mathrm{Ca}}_i = \frac{\mu_i|\widetilde{\mathbf{v}}_i|}{\sigma_{\mathbb{WO}}} \tag{19}$$

for phase $i = \mathbb{W}, \mathbb{O}$. *[4.1.0.3]* Note that $\sigma_{\mathbb{WO}}/\mu_i$ is a characteristic flow velocity that depends only on the fluid properties. *[4.1.0.4]* As a consequence the microscopic capillary number $\widetilde{\mathrm{Ca}}$ depends only on fluid properties, but is independent of the pore space properties.

*[4.1.1.1]* For a derivation of $\widetilde{\mathrm{Ca}}_i$ from the pore scale equations of motion, see [9, 32].

## V. **Macroscopic sample scale** $L$

*[4.1.2.1]* Consider again the stationary limit $t \to \infty$ of fluid flow in $\mathbb{P}$. *[4.1.2.2]* On the scale of a macroscopic sample, the viscous forces are dominated by wall friction and quantified by Darcy's law for single phase flow

$$v_{\mathrm{D}} = \phi v = \frac{k}{\mu}\frac{\mathrm{d}P}{L}, \tag{20}$$

where $v_{\mathrm{D}}$ is the magnitude of the (superficial) Darcy velocity, $v = |\mathbf{v}|$ is the phase velocity of the (interstitial) fluid, and $\mathrm{d}P$ is the magnitude of the viscous pressure drop across a region of length $L$. *[4.1.2.3]* Here $\mu$ is the fluid viscosity, $k$ is the (absolute) permeability and $\phi$ the porosity of the porous medium.

*[4.1.3.1]* The generalization of Darcy's law to two immiscible fluids requires some assumptions. *[4.1.3.2]* Let $\mathbb{W}(t_0)$, $\mathbb{O}(t_0)$ denote the fluid configuration inside the porous medium at some initial time $t_0$ and consider flooding at constant injection rates $Q_{\mathbb{W}} \neq 0, Q_{\mathbb{O}} = 0$ or $Q_{\mathbb{W}} = 0, Q_{\mathbb{O}} \neq 0$ with water or oil. *[4.1.3.3]* It is observed experimentally and then assumed theoretically that for long times $t \to \infty$ the total volume fractions

$$\lim_{t\to\infty}\frac{|\mathbb{W}(t)|}{|\mathbb{P}|} = \lim_{t\to\infty} S_{\mathbb{W}}(t) = S_{\mathbb{W}} = S \tag{21a}$$

$$\lim_{t\to\infty}\frac{|\mathbb{O}(t)|}{|\mathbb{P}|} = \lim_{t\to\infty} S_{\mathbb{O}}(t) = S_{\mathbb{O}} = 1 - S \tag{21b}$$

approach constant limiting values. *[4.2.0.4]* The values of $S_{\mathbb{W}}$, $S_{\mathbb{O}}$ will depend on the phase pressures $P_{\mathbb{W}}$, $P_{\mathbb{O}}$. *[4.2.0.5]* Because the injection rates are constant the homogenized phase velocities $\mathbf{v}_{\mathbb{W}}(t)$, $\mathbf{v}_{\mathbb{O}}(t)$ approach constant values. *[4.2.0.6]* Specifically,

$$\lim_{t\to\infty}|\mathbf{v}_{\mathbb{W}}(t)| = v_{\mathbb{W}}, \quad \text{and} \quad \lim_{t\to\infty}|\mathbf{v}_{\mathbb{O}}(t)| = 0 \tag{22a}$$

$$\lim_{t\to\infty}|\mathbf{v}_{\mathbb{W}}(t)| = 0, \quad \text{and} \quad \lim_{t\to\infty}|\mathbf{v}_{\mathbb{O}}(t)| = v_{\mathbb{O}} \tag{22b}$$

because $Q_{\mathbb{W}} \neq 0$, $Q_{\mathbb{O}} = 0$ for water flooding and $Q_{\mathbb{W}} = 0$, $Q_{\mathbb{O}} \neq 0$ for oil flooding. *[4.2.0.7]* Under these assumptions Darcy's law is generalized from single phase flow to two-phase flow as discussed in [33–37] to

$$v_{\mathrm{D}} = \phi v_i = \frac{k\,k_i^r(S)}{\mu_i}\frac{\mathrm{d}P_i}{L} \tag{23}$$

where $i = \mathbb{W}, \mathbb{O}$ indicates the two phases and the relative permeability functions $k_{\mathbb{W}}^r(S)$, $k_{\mathbb{O}}^r(S)$ quantify the change in permeability for phase $i$ due to presence of the second phase. *[4.2.0.8]* Note that the asymptotic water configuration $\mathbb{W}(\infty)$ must be path connected and percolating from inlet and outlet[†]in case (22a) and the same holds for $\mathbb{O}(\infty)$ in case (22b).

*[4.2.1.1]* The asymptotic pressure difference $P_{\mathbb{O}}(t) - P_{\mathbb{W}}(t)$ for $t \to \infty$ reflects microscopic capillarity on macroscales. *[4.2.1.2]* The difference is assumed to depend only on saturation

$$\lim_{t\to\infty}(P_{\mathbb{O}}(t) - P_{\mathbb{W}}(t)) = P_{\mathrm{c}}(S) = P_{\mathrm{b}}\,\widehat{P_{\mathrm{c}}}(S) \tag{24}$$

but not on the phase velocities although dynamic capillary effects have been observed [38, 39]. *[4.2.1.3]* The function $P_{\mathrm{c}}(S)$ is called capillary pressure and $\widehat{P_{\mathrm{c}}}(S)$ is its dimensionless form. *[4.2.1.4]* The functions $P_{\mathrm{c}}(S)$ and $k_i^r(S)$ are defined on the interval $[S_{\mathbb{W}\mathrm{i}}, 1 - S_{\mathbb{O}\mathrm{r}}]$. *[4.2.1.5]* The parameters $S_{\mathbb{W}\mathrm{i}}$, $S_{\mathbb{O}\mathrm{r}}$, defined as solutions of the equations

$$k_{\mathbb{W}}^r(S_{\mathbb{W}\mathrm{i}}) = 0 \tag{25a}$$

$$k_{\mathbb{O}}^r(1 - S_{\mathbb{O}\mathrm{r}}) = 0, \tag{25b}$$

are the irreducible water saturation $S_{\mathbb{W}\mathrm{i}}$ and the residual oil saturation $S_{\mathbb{O}\mathrm{r}}$. *[4.2.1.6]* Both parameters $S_{\mathbb{W}\mathrm{i}}$ and $S_{\mathbb{O}\mathrm{r}}$ are assumed to be small but nonvanishing, i.e. $0 < S_{\mathbb{W}\mathrm{i}} \ll 1$ and $0 < S_{\mathbb{O}\mathrm{r}} \ll 1$. *[4.2.1.7]* With $S_{\mathbb{W}\mathrm{i}}$ and $S_{\mathbb{O}\mathrm{r}}$ the parameter $P_{\mathrm{b}}$ in eq. (24) is defined as

$$P_{\mathrm{b}} = P_{\mathrm{c}}\left(\frac{S_{\mathbb{W}\mathrm{i}} + 1 - S_{\mathbb{O}\mathrm{r}}}{2}\right). \tag{26}$$

*[page 5, §0]* *[5.1.0.1]* If there is hysteresis, so that the values $P_{\mathrm{b}}^{\mathrm{im}} \neq P_{\mathrm{b}}^{\mathrm{dr}}$ differ, then $P_{\mathrm{b}} = (P_{\mathrm{b}}^{\mathrm{im}} + P_{\mathrm{b}}^{\mathrm{dr}})/2$ will be used. *[5.1.0.2]* The dimensionless capillary pressure function $\widehat{P_{\mathrm{c}}}(S)$ can be positive and negative. *[5.1.0.3]* The relative permeabilities are positive and monotone functions.

*[5.1.1.1]* The force balance between the viscous and capillary forces of macroscale two-phase flow can now be expressed

[†]Limitations and previously unnoticed implicit assumptions for the validity of (23) were first addressed in [15] and then formulated mathematically and explicitly as the residual decoupling approximation in [18–20].

either as a function of $S$, $v_i$ and $L$

$$F_i(S,v_i,L) = \frac{\text{(viscous pressure drop in phase } i)}{\text{(capillary pressure)}}$$
$$= \frac{|\mathrm{d}P_i|}{|P_{\mathbb{O}} - P_{\mathbb{W}}|} \tag{27a}$$
$$= \frac{\mu_i\,\phi\,v_i\,L}{k\,k_i^r(S)|P_{\mathrm{c}}(S)|} \tag{27b}$$
$$= \frac{\mathrm{Ca}_i}{k_i^r(S)\left|\widehat{P_{\mathrm{c}}}(S)\right|} \tag{27c}$$
$$= f_i(S,\mathrm{Ca}_i) \qquad i = \mathbb{W},\mathbb{O} \tag{27d}$$

or as a function of $S$ and the macroscopic capillary number $\mathrm{Ca}_i$ in the last two equalities. *[5.1.1.2]* The macroscopic capillary number $\mathrm{Ca}_i$ is defined as in [9] by

$$\mathrm{Ca}_i = \frac{\mu_i\,\phi\,v_i\,L}{k\,P_{\mathrm{b}}} \qquad i = \mathbb{W},\mathbb{O} \tag{28}$$

and it depends not only on fluid properties, but also on properties of the porous medium such as porosity and permeablity. *[5.1.1.3]* Equation (27) seems to be a new result that has been overlooked so far. *[5.1.1.4]* Note that Ca does not explicitly depend on the interfacial tension $\sigma_{\mathbb{WO}}$ between the two phases and that the quantity $A_i = k\,P_{\mathrm{b}}/(\mu_i\,\phi)$ with $i = \mathbb{W},\mathbb{O}$ is dimensionally not a velocity, but a specifc action, i.e. action per unit mass. *[5.1.1.5]* For a derivation of $\mathrm{Ca}_i$ from the traditional macroscale equations of motion see [9, 32].

## VI. Mesoscopic cluster scale $L_{\mathrm{cl}}$

*[5.1.2.1]* As of today there does not seem to exist a rigorous connection between the microscopic Newton and Laplace law and the macroscopic generalized Darcy law. *[5.1.2.2]* This fact was discussed at length in [9,16,17,20,32,40] and it is the reason why the microscopic interfacial tension $\sigma_{\mathbb{WO}}$ does not appear explicitly in the macroscopic capillary number in eq. (28). *[5.1.2.3]* Nevertheless numerous authors have mingled pore and sample scale in an attempt to discuss nonpercolating fluid parts, mesoscopic clusters or trapped ganglia. *[5.1.2.4]* A classic example, that led to some confusion, is given in [41] where Darcy's law for single phase flow (20) is inserted into eq. (19) to write

$$\widetilde{\mathrm{Ca}}_i^{\mathrm{OPC}} = \frac{k\,\mathrm{d}P_i}{\sigma_{\mathbb{WO}}\phi\,L} \qquad i = \mathbb{W},\mathbb{O} \tag{29}$$

replacing velocity and viscosity by permeability, porosity and pressure gradient. *[5.1.2.5]* Subsequently [4, eq. (9)] used the generalized Darcy law eq. (23) in eq. (19) to obtain

$$\widetilde{\mathrm{Ca}}_i^{\mathrm{MB}} = \frac{k\,k_i^r(S)\,\mathrm{d}P_i}{\sigma_{\mathbb{WO}}\,\phi\,L_{\mathrm{cl}}} \qquad i = \mathbb{W},\mathbb{O} \tag{30}$$

a pore-scale capillary "number" that is now a function of saturation $S$. *[5.1.2.6]* They then interpret this expression as a saturation dependent "critical" capillary number for mobilization of trapped oil ganglia with linear extent $L_{\mathrm{cl}}$. *[5.2.0.7]* Solving for $L_{\mathrm{cl}}$ gives $L_{\mathrm{cl}} = L_{\mathrm{cl}}(S,\widetilde{\mathrm{Ca}}_i)$. *[5.2.0.8]* Such approaches were critically examined in [9, 32, 40]. *[5.2.0.9]* The problem with eq. (30) emerges by noting that the same relation (30) can be obtained from the equality between the expression in (27a) and expression (27b) by using eq. (24) and multiplying with $1/\sigma_{\mathbb{WO}}$. *[5.2.0.10]* This derivation shows that the influence of $P_{\mathrm{c}}(S)$ on $L_{\mathrm{cl}}(S)$ is lost. *[5.2.0.11]* More importantly, it is clear from eqs. (22a) and (22b) that the generalized Darcy law requires pathconnected and percolating phases. *[5.2.0.12]* Its application to disconnected trapped phases is questionable at least as long as cross terms are not included into the analysis [42, 43]. *[5.2.0.13]* This casts some doubt on the interpretation of $L \approx L_{\mathrm{cl}}$ as a length scale of clusters.

*[5.2.1.1]* More recently this cluster length $L_{\mathrm{cl}}$ was discussed using Ca instead of $\widetilde{\mathrm{Ca}}$ in [5] following [40]. *[5.2.1.2]* The idea is to assume that mesoscopic (nonpercolating) clusters or trapped ganglia are roughly of size

$$L_{\mathrm{cl}} \approx L_i(S,v_i) = \frac{k\,k_i^r(S)|P_{\mathrm{c}}(S)|}{\mu_i\,\phi\,v_i}, \quad i = \mathbb{W},\mathbb{O} \tag{31}$$

where the length scale $L_i(S,v_i)$ is obtained from the macroscopic force balance by setting $F_i(S,v_i,L) = 1$ in eq. (27). *[5.2.1.3]* The capillary correlation from [5, eq. (7)] is defined following eq. (27b) as ($i = \mathbb{W},\mathbb{O}$)

$$\mathrm{Ca}_i^{\mathrm{AGOKB}} = \frac{\mu_i\,\phi\,v_i\,L_{\mathrm{cl}}(S,v,\mathbf{\Pi})}{k^{**}(S,v,\mathbf{\Pi})\,{P_{\mathrm{c}}}^{**}(S,v,\mathbf{\Pi})} \tag{32}$$

by replacing the macroscopic length $L$ with the mesoscopic $L_{\mathrm{cl}}$, the effective permeability $k\,k_i^r(S)$ with a computed permeability $k^{**} = k^{**}(S,v,\mathbf{\Pi})$ and the macroscopic capillary pressure $|P_{\mathrm{c}}(S)|$ with a computed pore scale capillary pressure ${P_{\mathrm{c}}}^{**} = {P_{\mathrm{c}}}^{**}(S,v,\mathbf{\Pi})$. *[5.2.1.4]* The quantities $k^{**}$ and ${P_{\mathrm{c}}}^{**}$ are obtained from pore scale imaging of $\mathbb{P}$, $\mathbb{W}$ and $\mathbb{O}$ by computations based on digital image analysis. *[5.2.1.5]* Their values depend on numerous numerical and computational parameters summarized as $\mathbf{\Pi}$. *[5.2.1.6]* Examples are segementation thresholds, lattice constants or density functional parametrizations used by [5] to replace more conventional computational fluid dynamics approaches. *[5.2.1.7]* Within the limits of applicability of the macroscopic constitutive laws (23) and (24) such computational approaches are expected to yield

$$k^{**}(S,v,\mathbf{\Pi}) \approx k\,k_i^r(S) \tag{33a}$$
$$P_{\mathrm{c}}{}^{**}(S,v,\mathbf{\Pi}) \approx P_{\mathrm{c}}(S) \tag{33b}$$

independent of $v$ and $\mathbf{\Pi}$. *[5.2.1.8]* If this holds true, then inserting eq. (31) is expected to give

$$\mathrm{Ca}_i^{\mathrm{AGOKB}} \approx 1 \tag{34}$$

provided $L_{\mathrm{cl}} \approx L_i(S,v_i)$ holds true. *[5.2.1.9]* Measuring the cluster length $L_{\mathrm{cl}}$ from fast X-ray computed microtomography [5, Fig. 1] finds values of

$$\mathrm{Ca}_i^{\mathrm{AGOKB}} \approx 10 \tag{35}$$

from saturation weighted averaging of the cluster size distribution.

*[5.2.2.1]* Note also, that the length scale $L_i(S,v_i)$ may often fall in between $\ell$ and $L$, but it can also exceed beyond these limits. *[5.2.2.2]* In fact $0 \leq L_i < \infty$ in general. *[5.2.2.3]* The length scale $L_i$ cannot be considered a new mesoscopic

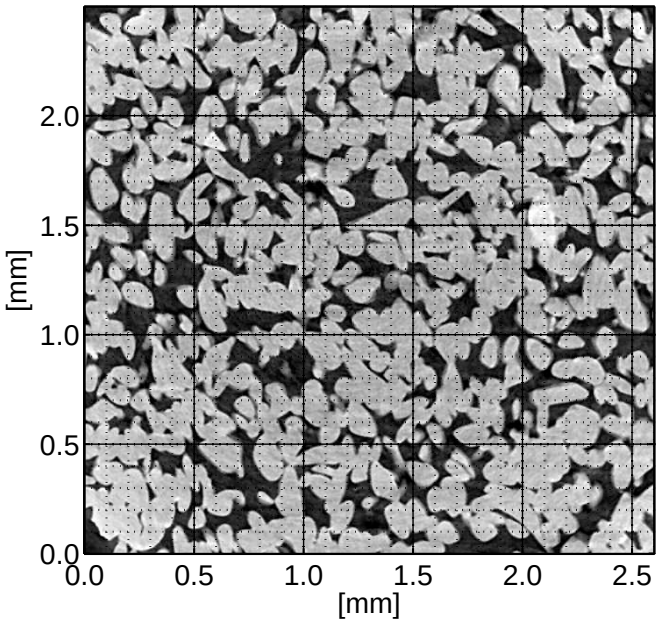


FIGURE 1. Cross section of 2.6mm×2.5mm (632×607 pixel, 16 bit gray values) at $4.1\mu$m resolution from a 3-dimensional computertomographic image of a VitraPOR P2 Robu® sintered glass specimen. Matrix $\mathbb{M}$ is shown in grey, pores $\mathbb{P}$ are black.

length scale, because it is not derived from a new mesoscopic constitutive law. *[page 6, §0]* *[6.1.0.1]* Mesoscopic laws for $L_{\rm cl}$ defined as the saturation weighted average of the distribution of cluster sizes, are also lacking at present. *[6.1.0.2]* Although constitutive laws for disconnected fluids have been proposed in [19] and discussed in [21] the present article will stay within the confines of the traditional Darcy based constitutive theory.

## VII. Application to experiment

### A. Definition of desaturation protocols

*[6.1.1.1]* As emphasized above (see also footnote †) the validity of the generalized Darcy law (23) requires path connected fluids, i.e. fluid configurations that percolate from inlet to outlet. *[6.1.1.2]* Application of $\mathrm{Ca}_i$ from (28) to water flooding desaturation experiments therefore requires that also the oil configuration $\mathbb{O}(t_0)$ is percolating at the initial time $t_0$, if the generalized Darcy law is assumed to describe the reduction of oil saturation. *[6.1.1.3]* An appropriate desaturation protocol consists of $M$ steps with

$$\mathbb{O}(t_{k-1}) = \mathbb{P}, \tag{36a}$$
$$\mathbb{W}(t_{k-1}) = \emptyset, \tag{36b}$$
$$Q_{\mathbb{O}}(t) = 0, \qquad t_{k-1} \le t \le t_k \tag{36c}$$
$$Q_{\mathbb{W}}(t) = Q_k\, \chi_{[t_{k-1},t_k]}(t), \qquad t_{k-1} \le t \le t_k \tag{36d}$$

with $1 \le k \le M$ and $t_k$ is chosen such that

$$[t_{k-1}, t_k] \setminus \operatorname{supp} O_{\mathbb{O}}(t) \neq \emptyset, \tag{37}$$

holds for every fixed $k$. *[6.1.1.4]* Here $Q_k$ are constant and $O_{\mathbb{O}}(t)$ denotes the volumetric production rate (outflow) of oil. Its support $\operatorname{supp} O_{\mathbb{O}}(t)$ is the set of time instants $t \in \mathbb{R}$ for which $O_{\mathbb{O}}(t) \neq 0$ holds. *[6.2.0.5]* Condition (37) means that the oil production has stopped. *[6.2.0.6]* During the experiment the oil phase is kept at a sufficiently high ambient pressure so that, depending on the pressure drop across the sample, also oil can enter the sample during the water flood. *[6.2.0.7]* The desaturation protocol (36) is a continuous mode displacement where water is injected into continuous oil. *[6.2.0.8]* It will be referred to as CO/WI for short.

*[6.2.1.1]* The CO/WI-protocol (36) requires to clean the sample after each step and refill it with oil. *[6.2.1.2]* This is costly and time consuming. *[6.2.1.3]* Many capillary desaturation experiments are therefore performed in discontinuous mode. *[6.2.1.4]* In discontinuous mode the water injection rate $Q_{\mathbb{W}}$ is increased in steps, and the initial configuration of step $k$ is the final configuration of step $k-1$. *[6.2.1.5]* The initial oil configuration $\mathbb{O}(t_0)$ may or may not be percolating. *[6.2.1.6]* The desaturation protocol

$$\mathbb{O}(t_{k-1}) = \text{arbitrary}, \qquad 1 \le k \le M \tag{38a}$$
$$\mathbb{W}(t_{k-1}) = \text{arbitrary}, \qquad 1 \le k \le M \tag{38b}$$
$$Q_{\mathbb{O}}(t) = 0, \qquad t_{k-1} \le t \le t_k \tag{38c}$$
$$Q_{\mathbb{W}}(t) = Q_k\, \chi_{[t_{k-1},t_k]}(t), \qquad t_{k-1} \le t \le t_k \tag{38d}$$
$$Q_k \le Q_{k+1}, \qquad 1 \le k \le M-1 \tag{38e}$$

will be referred to as DO/WI (discontinuous oil/water injection). *[6.2.1.7]* Here $t_k$ is again chosen such that condition (37) holds i.e. one waits sufficiently long until the oil production $O_{\mathbb{O}}(t)$ after step $k-1$ has ceased. *[6.2.1.8]* For nonpercolating fluid configurations the applicability of eq. (23) and (28) is in doubt as emphasized in [40] and known from experiment [10].

*[6.2.2.1]* To exclude gravity effects the water flow direction is usually oriented perpendicular to gravity. *[6.2.2.2]* In addition the sample's thickness parallel to gravity is chosen much smaller than the width of the capillary fringe $\ell_{\mathbb{W}} = P_{\rm b}/(\varrho_{\mathbb{W}} g)$ where $\varrho_{\mathbb{W}}$ is the mass density of water and $g$ the acceleration of gravity to minimize saturation gradients due to gravity.

*[6.2.3.1]* Finally, a new protocol, introduced in [5], is used for application to experiment in the next section. *[6.2.3.2]* In [5] the cylindrical sample was oriented vertically, parallel to the direction of gravity in contradistinction to the conventional setup. *[6.2.3.3]* The wetting fluid was injected from the bottom against the direction of gravity. *[6.2.3.4]* The sample was always wetted by a water reservoir at the top. *[6.2.3.5]* The water pressure in the top reservoir was increasing during the experiment due to water accumulation. *[6.2.3.6]* A period of water injection was followed by a period of imaging the fluid distributions. *[6.2.3.7]* The new injection protocol resulting

from these procedures is defined as

$$|\mathbb{O}(t_0)| = (1 - S_{\mathbb{W}\mathrm{i}})\,|\mathbb{P}| \tag{39a}$$
$$|\mathbb{W}(t_0)| = S_{\mathbb{W}\mathrm{i}}\,|\mathbb{P}| \tag{39b}$$
$$\mathbb{O}(t_{k-1}) = \text{arbitrary}, \qquad 1 \le k \le M \tag{39c}$$
$$\mathbb{W}(t_{k-1}) = \text{arbitrary}, \qquad 1 \le k \le M \tag{39d}$$
$$Q_{\mathbb{O}}(t) = 0 \qquad t_{k-1} \le t \le t_k \tag{39e}$$
$$Q_{\mathbb{W}}(t) = Q_k\,\chi_{[t_{k-1},t_k]}(t), \qquad t_{k-1} \le t \le t_k \tag{39f}$$
$$Q_{2k} = 0, \qquad 1 \le k \le M/2 \tag{39g}$$
$$Q_{2k-1} \le Q_{2k+1}, \qquad 1 \le k \le M/2 \tag{39h}$$

*[page 7, §0]* where $t_{2k+1}$ is chosen subject to condition (37). *[7.1.0.1]* This protocol will be referred to as DO/IWI/G standing for discontinuous oil/interrupted water injection/gravity. *[7.1.0.2]* Note, however, that the oil configuration was typically percolating at $t = t_0$. *[7.1.0.3]* During the imaging intervals $[t_{2k-1}, t_{2k}]$ resaturation and relaxation processes may have changed the original fluid configuration and saturation as compared to the instant when the pump was switched off.

## B. Application to mesoscopic experiments [5]

*[7.1.1.1]* This section applies concepts and results from the preceding sections to recent highly advanced capillary desaturation experiments with simultaneous fast X-ray computed microtomography [5]. *[7.1.1.2]* The experiments in [5] used the DO/IWI/G-protocol defined in (39). *[7.1.1.3]* The experiment had $M = 5$ steps with

$$Q_k = 10^{k-2}\ \mu\mathrm{L/min} = 1.6666 \times 10^{k-13}\ \mathrm{m^3 s^{-1}} \tag{40}$$
$$v_{\mathbb{W}k} = \frac{Q_k}{\phi A_{\mathbb{S}}} = 4.17 \times 10^{k-8}\ \mathrm{ms^{-1}}. \tag{41}$$

as injection rates, respectively phase velocities. *[7.1.1.4]* After reaching stationary water flow without oil production, the nonwetting phase saturations remaining inside the sample were measured and found to be $S_{\mathbb{O}_1} = 0.75$, $S_{\mathbb{O}_2} = 0.75$, $S_{\mathbb{O}_3} = 0.5$, $S_{\mathbb{O}_4} = 0.3$, $S_{\mathbb{O}_5} = 0.2$.

*[7.1.2.1]* The experiments were performed on sintered borosilicate glass commercially available as VitraPOR P2 from ROBU Glasfilter Geräte GmbH (Hattert, Germany). *[7.1.2.2]* A quadratic cross section of this porous medium with a sidelength of 2.6 mm is shown in Figure 1 to illustrate its pore structure. *[7.1.2.3]* The pore structure is less homogeneous than that of certain natural sandstones often used for pore scale and core scale studies. *[7.1.2.4]* A cylindrical specimen

$$\mathbb{S} = [0, L] \times \{x \in \mathbb{R}^2 : |x| \le d\} \tag{42}$$

of this porous medium with diameter

$$d = 0.02523\ \mathrm{m}, \tag{43a}$$

length

$$L = 0.08778\ \mathrm{m} \tag{43b}$$

and total volume $|\mathbb{S}| = 4.3885 \times 10^{-5}\ \mathrm{m^3}$ was measured to have a pore volume of $|\mathbb{P}| = 1.4090 \times 10^{-5}\ \mathrm{m^3}$ and a grain volume of $|\mathbb{M}| = 2.9795 \times 10^{-5}\ \mathrm{m^3}$. *[7.1.2.5]* Its porosity and Klinkenberg corrected air permeability

$$\phi = 0.321 \tag{44a}$$
$$k = 8.952 \times 10^{-12}\ \mathrm{m^2} \tag{44b}$$

correspond to a well permeable, medium to coarse grained sandstone. *[7.1.2.6]* Mercury injection porosimetry was performed on this sample. *[7.1.2.7]* It showed a breakthrough pressure of $P_{\mathrm{b}}^{\mathrm{Hg}} \approx 2584$ Pa resulting in a typical pore size of roughly 56 $\mu$m if

$$\sigma_{\mathrm{Hg}} = 0.48\ \mathrm{Nm^{-1}} \tag{45a}$$
$$\vartheta_{\mathrm{Hg}} = 139^\circ \tag{45b}$$

are used for the surface tension and contact angle of mercury. *[7.2.0.8]* The capillary desaturation experiments in [5] were performed using $n$-decane as the nonwetting fluid $\mathbb{O}$ and water with CsCl as contrast agent as the wetting fluid $\mathbb{W}$. *[7.2.0.9]* The mercury pressures can be rescaled with

$$\sigma_{\mathbb{WO}} = 0.03\ \mathrm{Nm^{-1}} \tag{46a}$$
$$\vartheta_{\mathbb{WO}} \approx 35^\circ \tag{46b}$$

to the water/$n$-decane system according to

$$P_{\mathrm{c}}(S) = \frac{\sigma_{\mathbb{WO}}\cos(\vartheta_{\mathbb{WO}})}{\sigma_{\mathrm{Hg}}\cos(\vartheta_{\mathrm{Hg}})} P_{\mathrm{c}}{}^{\mathrm{Hg}}(S) \tag{47}$$

if Leverett-J-function scaling is assumed to to be valid. *[7.2.0.10]* The rescaled mercury drainage pressure function in the range up to 3086 Pa is shown in the upper part of Figure 2 with crosses. *[7.2.0.11]* For subsequent computations the imbibition curve and the relative permeabilties shown in Figure 2 had to be assumed theoretically, because experimental data were not available. *[7.2.0.12]* The particular choice for their functional form will influence the numerical results, but is not important for our theoretical argument. *[page 8, §0]* *[8.1.0.1]* The fluid viscosities were

$$\mu_{\mathbb{W}} = 0.89 \times 10^{-3}\ \mathrm{Pas} \tag{48a}$$
$$\mu_{\mathbb{O}} = 3.0 \times 10^{-3}\ \mathrm{Pas}. \tag{48b}$$

for water denoted $\mathbb{W}$ and $n$-decane denoted as $\mathbb{O}$.

*[8.1.1.1]* The capillary desaturation experiments in [5] were performed not on the full sample $\mathbb{S}$, but on a small subset of $\mathbb{S}$. *[8.1.1.2]* That cylindrical subsample had

$$d = 0.004\ \mathrm{m} \tag{49a}$$
$$L = 0.01\ \mathrm{m} \tag{49b}$$
$$A_{\mathbb{S}} = 1.26 \times 10^{-5}\ \mathrm{m^2} \tag{49c}$$

where $A_{\mathbb{S}}$ denotes the cross sectional area[‡].

*[8.1.2.1]* The resulting microscopic capillary numbers were[§]

$$\widetilde{\mathrm{Ca}}_{\mathbb{W}k} = \frac{\mu_{\mathbb{W}} v_{\mathbb{W}k}}{\sigma_{\mathbb{WO}}} = 1.23 \times 10^{k-9} \tag{50}$$

[‡]Assuming perfect isotropy the dimensionless aspect ratio matrix becomes diagonal with $\widehat{\mathbf{A}} = \mathrm{diag}(1.99, 1.99, 0.25)$ according to eq. (28) in [40]. Because of the ratio of $A_{xx}/A_{zz} \approx 8$ it should be kept in mind that geometric factors can change the force balance by an order of magnitude.

[§]These capillary numbers differ from those shown in Figure 1 of [5] by a factor $\phi$.

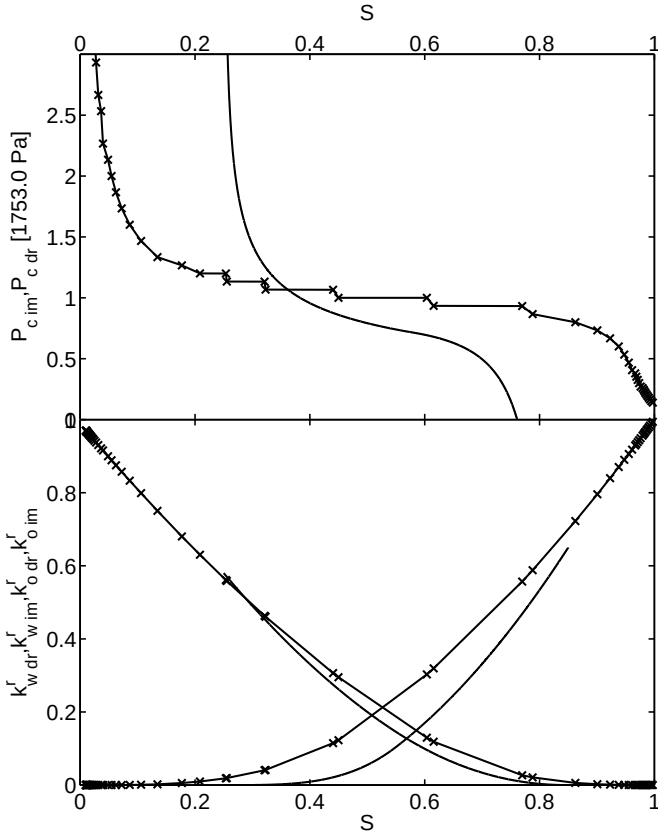


FIGURE 2. Capillary pressure $P_{\mathrm{c}\,j}(S)$ and relative permeabilities $k^{\mathrm{r}}_{i\,j}(S)$ for drainage (symbols, $j$ =dr) and imbibition (smooth solid, $j$ =im) $i = \mathbb{W}, \mathbb{O}$. The capillary pressure for drainage is obtained from mercury porosimetry on VitraPOR P2 by rescaling according to eq. (47) with a Leverett-J-function Ansatz. The imbibtion curve and all relative permeabilities shown were specified theoretically, because experimental data were not available. Their values shown here are typical and were used in all computations.

with $k = 1, 2, 3, 4, 5$. *[8.1.2.2]* To compute the macroscopic capillary number from (28) the characteristic pressure $P_{\mathrm{b}}$ is taken from the rescaled drainage curve in the upper part of Figure 2 as

$$P_{\mathrm{b}} \approx 1753 \text{ Pa}. \tag{51}$$

*[8.1.2.3]* With this the macroscopic capillary numbers for the $L = 8.778$ cm-sample are

$$\mathrm{Ca}_{\mathbb{W}k} = \frac{\mu_{\mathbb{W}}\,\phi\,v_{\mathbb{W}}\,L}{k\,P_{\mathrm{b}}} \approx 6.60 \times 10^{k-5} \tag{52}$$

for $k = 1, 2, 3, 4, 5$, while

$$\mathrm{Ca}_{\mathbb{W}k} = 7.52 \times 10^{k-6} \tag{53}$$

for the 1 cm-sample. *[8.1.2.4]* Note, that the width $\ell_{\mathbb{W}}$ of the capillary fringe of water

$$\ell_{\mathbb{W}} = \frac{P_{\mathrm{b}}}{\varrho_{\mathbb{W}} g} \approx 0.179 \text{ m} \tag{54}$$

is around 18 cm, where $\varrho = 1000\ \mathrm{kgm}^{-3}$ is the density of water and $g$ is the acceleration of gravity.

*[8.1.3.1]* Figure 3 compares the experimental observations to the theoretical predictions. *[8.1.3.2]* Assuming $L$ to be fixed, the theoretically predicted capillary desaturation curve $S_{\mathbb{O}}(\mathrm{Ca}_{\mathbb{W}}; F)$ for fixed force balance $F$ is obtained from the solution $S(\mathrm{Ca}_{\mathbb{W}}; F)$ of eq. (27)

$$F = f_{\mathbb{W}}(S, \mathrm{Ca}_{\mathbb{W}}) \tag{55}$$

as $S_{\mathbb{O}}(\mathrm{Ca}_{\mathbb{W}}; F) = 1 - S(\mathrm{Ca}_{\mathbb{W}}; F)$. *[8.1.3.3]* Figure 3 shows two capillary desaturation curves $S_{\mathbb{O}}(\mathrm{Ca}_{\mathbb{W}}; 1)$ for water injection into continuous oil according to the CO/WI-protocol (36). *[8.1.3.4]* One curve (crosses) represents drainage, while the solid curve represents imbibition. *[8.2.0.5]* Crosses are computed using the rescaled mercury drainage pressures and relative permeabilities for drainage shown in Fig. 2. *[8.2.0.6]* The solid curve without symbols is computed from the imbibition curves in Fig. 2. *[8.2.0.7]* The values of $S_{\mathbb{O}\,\mathrm{r}} = 0.15$ and $1 - S_{\mathbb{W}\,\mathrm{i}} = 0.75$ are indicated by dashed horizontal lines.

*[8.2.1.1]* If all assumptions underlying the traditional equations and the derivations of $S_{\mathbb{O}}(\mathrm{Ca}_{\mathbb{W}}; F)$ hold true, then the experimental results are expected to fall in between the two limiting drainage and imbibition curves. *[8.2.1.2]* To test this expectation Figure 3 shows three experimental capillary desaturation correlations. *[8.2.1.3]* The experimental values $S_{\mathbb{O}_k}$ with $k = 1, 2, 3, 4, 5$ are plotted as squares against $\widetilde{\mathrm{Ca}}_{\mathbb{W}\,k}$ from eq. (50), as triangles against $\mathrm{Ca}_{\mathbb{W}\,k}$ from eq. (53), and as circles against $\mathrm{Ca}_{\mathbb{W}\,k}$ from eq. (52). *[8.2.1.4]* This comparison between theory and experiment rules out the use of microscopic capillary number $\widetilde{\mathrm{Ca}}_{\mathbb{W}\,k}$ as abscissa in capillary desaturation curves. *[8.2.1.5]* The misleading use of this number is still widely spread in current literature although it has been criticized already in [9, 32]. *[8.2.1.6]* The comparison with $\mathrm{Ca}_{\mathbb{W}\,k}$ confirms the predictions of traditional two phase flow theory as far as orders of magnitude are concerned. *[8.2.1.7]* However, it must be emphasized that the comparison uses the CO/WI-protocol for theory, but the DO/IWI/G-protocol for experiment. *[8.2.1.8]* The theoretical predictions restrict capillary desaturation curves to the region $\mathrm{Ca}_{\mathbb{W}} < 1$. *[8.2.1.9]* This prediction is a consequence of the fact that the traditional theory cannot account for disconnected nonpercolating fluid parts. *[page 9, §0]* *[9.1.0.1]* Figure 3 represents, to the best of our knowledge, the first example in which bounds for capillary desaturation curves have been predicted based solely on the constitutive functions of the traditional two phase flow theory.

## C. Predictions for new experiments

*[9.1.1.1]* This subsection introduces for the first time continuous mode capillary saturation experiments in analogy to capillary desaturation experiments. *[9.1.1.2]* The new saturation

protocol is defined as

$$\mathbb{O}(t_{k-1}) = \mathbb{P}, \tag{56a}$$
$$\mathbb{W}(t_{k-1}) = \emptyset, \tag{56b}$$
$$Q_{\mathbb{O}}(t) = Q_k\ \chi_{[t_{k-1},t_k]}(t), \qquad t_{k-1} \le t \le t_k \tag{56c}$$
$$Q_{\mathbb{W}}(t) = 0, \qquad t_{k-1} \le t \le t_k \tag{56d}$$

where $1 \le k \le M$. *[9.1.1.3]* For each fixed $k$ the time $t_k$ is chosen such that

$$[t_{k-1}, t_k] \setminus \operatorname{supp} O_{\mathbb{W}}(t) \neq \emptyset, \tag{57}$$

holds, i.e. such that the water production has ceased. *[9.1.1.4]* The saturation protocol (56) will be referred to as CO/OI-protocol (continuous oil/oil injection). *[9.1.1.5]* To the best of our knowledge such capillary saturation experiments with CO/OI-protocol have not been performed.

*[9.1.2.1]* During the CO/OI-protocol the water phase is kept at a sufficiently high ambient pressure so that water can enter the sample while oil is injected. *[9.1.2.2]* If the ambient pressure is sufficiently high and the oil injection rates are small, the resulting displacement process is expected to show strongly interacting mesoscopic cluster dynamics with numerous breakup and coalescence processes of mesoscopic clusters.

*[9.1.3.1]* Applying the theoretical prediction from eq. (27) yields capillary saturation curves $S_{\mathbb{O}}(\mathrm{Ca}_{\mathbb{O}}; F)$ for fixed force balance $F$ from solutions $S(\mathrm{Ca}_{\mathbb{O}}; F)$ of the equation

$$F = f_{\mathbb{O}}(S, \mathrm{Ca}_{\mathbb{O}}) \tag{58}$$

as $S_{\mathbb{O}}(\mathrm{Ca}_{\mathbb{O}}; F) = 1 - S(\mathrm{Ca}_{\mathbb{O}}; F)$ analogous to capillary desaturation curves shown in Figure 3. *[9.1.3.2]* The theoretically predicted bounding capillary saturations curves $S(\mathrm{Ca}_{\mathbb{O}}; 1)$ for drainage (crosses) and imbibition (solid curve) are displayed in Figure 4 using again the function $P_{\mathrm{c}}, k^r_{\mathbb{W}}, k^r_{\mathbb{O}}$ shown in Figure 2. *[9.1.3.3]* Experiments following the CO/OI-protocol are expected to fall in between these two limiting curves. *[9.1.3.4]* Figure 4 shows that the region between the curves becomes narrow for $\mathrm{Ca}_{\mathbb{O}} \approx 0.1$ or $0.3 \le S_{\mathbb{O}} \le 0.7$ for the chosen parameters. *[9.1.3.5]* In this region strongly interacting mesoscopic clusters are expected to arise from strongly fluctuating breakup ond coalescence of oil ganglia. *[9.1.3.6]* This expectation is consistent with theoretical network modeling in [44] and with recent experimental observations of two temporal regimes of percolating and nonpercolating fluid flow during imbibition into Gildehauser sandstone in [45].

## VIII. Discussion

### A. Theoretical predictions

*[9.2.1.1]* This article has introduced theoretical predictions from eq. (27) shown in Figure 3 for continuous mode capillary desaturation that until now seem to have remained unnoticed within the established traditional theory of twophase flow. *[9.2.1.2]* The predictions illustrated in Figure 3 provide a quantitative basis to discuss deviations observed in capillary desaturation experiments. *[9.2.1.3]* They help to establish limits of validity for the traditional theory as well as for continuous mode desaturation. *[9.2.1.4]* Predictions require precise knowledge of $P_{\mathrm{c}}(S)$, $k^r_{\mathbb{W}}(S)$ and $k^r_{\mathbb{O}}(S)$ emphasizing the importance and need for reliable special core analysis of high quality.

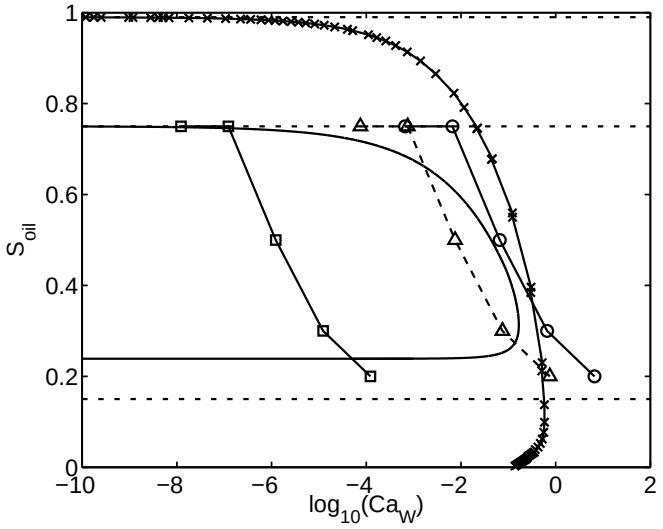


FIGURE 3. Two theoretical capillary desaturation curves $S_{\mathbb{O}}(\mathrm{Ca}_{\mathbb{W}}; 1)$ for water injection into continuous oil according to the CO/WI-protocol (36) with force balance $F = 1$. One curve (crosses) assumes drainage the other curve (solid) uses imbibition. The lower plateau value of the imbibition curve (solid) is given by the the zero of $P_{\mathrm{c}}{}^{\mathrm{imb}}$ (see eq. (60)). At this saturation $F = \infty$ diverges and below it $\mathrm{Ca}_{\mathbb{W}}$ cannot be expected to repesent the correct force balance (due to breakup of the nonwetting phase into disconnected ganglia). Crosses are computed using the rescaled mercury drainage pressures and relative permeabilities for drainage shown in Fig. 2. The solid curve without symbols is computed from the imbibition curves in Fig. 2. Also shown are three experimental capillary desaturation corrrelations plotting the experimental values $S_{\mathbb{O}_k}$ with $k = 1, 2, 3, 4, 5$ as squares against $\widetilde{\mathrm{Ca}}_{\mathbb{W}}$ from eq. (50), as triangles against $\mathrm{Ca}_{\mathbb{W}}$ from eq. (53), and as circles against $\mathrm{Ca}_{\mathbb{W}}$ from eq. (52).

### B. Protocol dependence

*[9.2.2.1]* The efficiency of residual oil recovery during waterflooding depends not only on the balance of forces, but also on other factors, such as the distribution of fluids inside the medium and/or the desaturation protocol. *[9.2.2.2]* The difference between continuous mode and discontinuous mode desaturation is known in the literature and it may change the critical capillary number (breakpoint) by several decades (see e.g. [40]). *[9.2.2.3]* The present paper suggests for the first time equally strong differences between the DO/IWI/G-protocol and the DO/WI-protocol. *[9.2.2.4]* For the latter protocol the breakpoint is sometimes found decades above unity. *[9.2.*

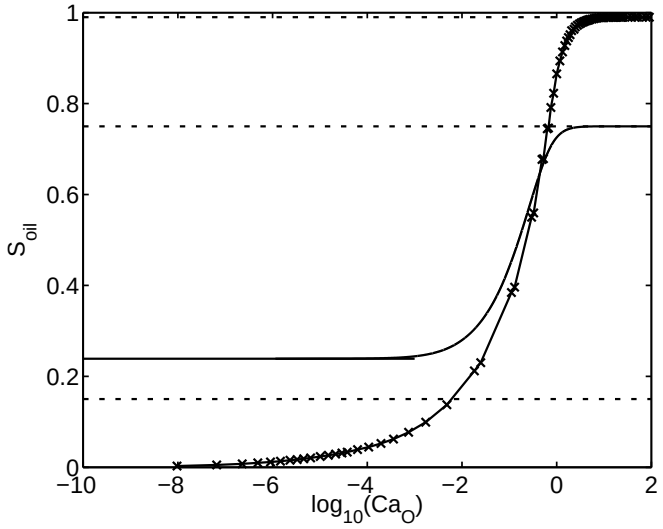


FIGURE 4. Theoretically predicted capillary saturation curves for oil injection into continuous oil according to the CO/OI-protocol (56) at $F = 1$. The curve with crosses corresponds to drainage, the solid line without symbols to imbibition.

*2.5]* Further studies of protocol dependence are encouraged to corroborate and clarify such differences and their origin.

## C. Plateau saturation

*[9.2.3.1]* If the saturation or desaturation process is experimentally reproducible one expects for the CO/WI- and CO/OI-protocols that *[page 10, §0]*

$$\mathbb{W}(t_i) \approx \mathbb{W}(t_j) \tag{59a}$$

$$|\mathbb{W}(t_i)| \approx |\mathbb{W}(t_j)| \tag{59b}$$

$$S(t_i) \approx S(t_j) \approx S^{\mathrm{p}} \tag{59c}$$

holds in the limit where $Q_i \to 0$ and $Q_j \to 0$ are both very small. *[10.1.0.1]* The saturation $S^{\mathrm{p}}$ denotes the plateau saturation. *[10.1.0.2]* It is seen from Figures 3 as well as 4 that the plateau saturation will in general differ from $S_{\mathbb{O}\,\mathrm{r}}$. *[10.1.0.3]* It fulfills either $S^{\mathrm{p}} \geq 1 - S_{\mathbb{W}\,\mathrm{i}}$ or $S^{\mathrm{p}} \leq S_{\mathrm{z}}$, where $S_{\mathrm{z}}$ is defined as the zero

$$P_{\mathrm{c}}{}^{\mathrm{imb}}(S_{\mathrm{z}}) = 0 \tag{60}$$

on the capillary pressure curve for secondary imbibition. *[10.1.0.4]* The actual value is expected to depend on the protocol.

## D. Computation of $P_{\mathrm{b}}$ from image analysis

*[10.1.1.1]* The stationary pore scale pressure fields $P_i(\widetilde{\mathbf{x}})$ ($i = \mathbb{W}, \mathbb{O}$) are generally assumed to represent equilibrium pressures for local thermodynamic equilibrium although the stationary phase velocities $v_i$ may be nonzero. *[10.1.1.2]* Even at $v_i = 0$ the pressures cannot be constant throughout the pore space $\mathbb{P}$, because curved interfaces exist in local thermodynamic equilibrium within $\mathbb{P}$.

*[10.1.2.1]* The macroscopic capillary pressure $P_{\mathrm{c}}(S, v)$ from eq. (24) measured in experiments for a sample with saturation $S$ at constant flow velocity $v$ is typically measured using pressure sensors located in the oil and water reservoirs outside the sample. *[10.1.2.2]* These pressure sensors average the local equilibrium pressure field $P_i(\widetilde{\mathbf{x}})$ over the surface $\partial\mathbb{D}$ of the sensor. *[10.1.2.3]* Assuming that the local equilibrium pressures $P_i(\widetilde{\mathbf{x}}; S)$ depend parametrically only on $S$, but are independent of $v$, one has

$$P_{\mathrm{c}}(S) = \frac{1}{|\partial\mathbb{D}_{\mathbb{O}}|} \int\limits_{\partial\mathbb{D}_{\mathbb{O}}} P_{\mathbb{O}}(\widetilde{\mathbf{x}}; S)\mathrm{d}^2\widetilde{\mathbf{x}} - \frac{1}{|\partial\mathbb{D}_{\mathbb{W}}|} \int\limits_{\partial\mathbb{D}_{\mathbb{W}}} P_{\mathbb{W}}(\widetilde{\mathbf{x}}; S)\mathrm{d}^2\widetilde{\mathbf{x}} \tag{61}$$

where $\partial\mathbb{D}_i$ denote the sensor surface located in the reservoir of phase $i$. *[10.1.2.4]* In [5] a pore scale capillary pressure $P_{\mathrm{c}}{}^{**}$ is computed from image analysis of oil clusters as a surface area weighted average of mean curvatures over the fluid-fluid-interface during the imaging intervals without flow ($v = 0$). *[10.1.2.5]* In other words a formula such as

$$P_{\mathrm{c}}{}^{**}(S,0,\mathbf{\Pi}; w) = \frac{\sigma_{\mathbb{W}\mathbb{O}}}{|\partial(\mathbb{W}\cap\mathbb{O})|} \int\limits_{\partial(\mathbb{W}\cap\mathbb{O})} w(\widetilde{\mathbf{x}})\kappa(\widetilde{\mathbf{x}})\mathrm{d}^2\widetilde{\mathbf{x}} \tag{62}$$

with a weighting function $w(\widetilde{\mathbf{x}})$ was used to estimate $P_{\mathrm{b}}$. *[10.2.0.6]* The weighting function is based on estimating the fluid/fluid interfacial area which in turn depends on the method and parameters of discretizing the interface. *[10.2.0.7]* Here $\kappa(\widetilde{\mathbf{x}})$ is the estimate of the local curvature of the interface. *[10.2.0.8]* The computed capillary pressures $P_{\mathrm{c}}{}^{**}(S, 0, \mathbf{\Pi}; w)$ reported in Figure 2(a) of [5] range between 250 Pa and 380 Pa. *[10.2.0.9]* This would suggest a value of

$$P_{\mathrm{b}}(\mathbf{\Pi}; w) = 315 \text{ Pa} \tag{63}$$

for the characteristic pressure $P_{\mathrm{b}}$. *[10.2.0.10]* We emphasize that clusters at much higher local $P_{\mathrm{c}}$ have been observed in the experiments. *[10.2.0.11]* The weighting function $w$ emphasizes the largest cluster and this cluster had very low mean curvature. *[10.2.0.12]* A precise mathematical relation between $P_{\mathrm{c}}$ and $P_{\mathrm{c}}{}^{**}$ cannot be given without a rigorous connection between the microscopic Newton and Laplace law and the macroscopic generalized Darcy law (cf. Section VI). *[10.2.0.13]* Equations (61) and (62) above do not establish such a connection because the domains of integration are disjoint, i.e. $\partial\mathbb{D}_i \cap \partial(\mathbb{W}\cap\mathbb{O}) = \emptyset$. *[10.2.0.14]* The derivation of macroscopic capillary properties of porous media expressed through $P_{\mathrm{c}}(S)$ from microscopic knowledge of the curvature field $\kappa(\widetilde{\mathbf{x}})$ remains a challenge.

## E. Cooperative dynamics and inertial effects

*[10.2.1.1]* Inertial effects and cooperative dynamics of mesoscaleclusters have been visualized using recent advances in X-ray microcomputed tomography synchrotron beamlines [46]. *[10.2.1.2]* The cooperative dynamics is believed to be related

to leading and trailing menisci connected via viscous pressure gradients. *[10.2.1.3]* These inertial effects are not visible on the scale of a single pore. *[10.2.1.4]* In a porous medium burst-type events are observed as reported by [47] or [48]. *[10.2.1.5]* In [46] it is shown that large events seem to be more frequent than suggested by simple percolation models¶. *[10.2.1.6]* While a single pore-scale event occurs over the millisecond time scale [50], i.e. displacement in a single pore, the occurrence of multiple spatially correlated events have been observed to decay over the second time scale [46]. *[10.2.1.7]* These observations might possibly indicate the emergence of a mesoscopic time or length scale intermediate between pore size $\ell$ and system size $L$. *[10.2.1.8]* Recent experimental evidence from [11] suggests that cluster lengths are flow rate dependent and widely distributed, ranging from many hundreds of pores down to a single pore. *[10.2.1.9]* If such a cluster length or other mesoscopic length and/or time scale exists, its upper and lower limits are unknown at present. *[10.2.1.10]* This challenges also the interpretation of laboratory-based results.

## IX. Conclusions

*[10.2.2.1]* This article has studied the process dependence of capillary desaturation curves $S(\mathrm{Ca})$ from the perspective of established theory and uncovered several new results. *[10.2.2.2]* It has introduced a mathematical expression for $S(\mathrm{Ca})$ in terms of relative permeabilities and normalized capillary pressure functions that has apparently remained unnoticed so far. *[10.2.2.3]* The article confirms the analysis of the traditional equations of motion by [9,32] and accounts for all explicit and implicit dependencies during desaturation experiments within the limits of applicability of the generalized Darcy law and capillary pressure hypothesis. *[10.2.2.4]* The following new results have been obtained by combining Darcy's law with microscopic arguments. *[10.2.2.5]* Firstly, this article provides predictive bounds on capillary number correlations (capillary saturation curves) for oil injection experiments. *[page 11, §0]* *[11.1.0.1]* Secondly, it proposes new capillary saturation experiments with oil injection instead of water injection. *[11.1.0.2]* Thirdly, the suggested novel CO/OI-protocol is expected to be dominated by flow processes involving mesoscale cluster rearrangement. *[11.1.0.3]* This is expected to allow for an evaluation and improved understanding of the emergence or not of mesoscale behaviour with a new mescopic length scale. *[11.1.0.4]* Fourthly, eq. (27) introduces a relation between capillary desaturation curves and the product $k^r(S)P_\mathrm{c}(S)$ that seems to have remained unnoticed so far. *[11.1.0.5]* Fifthly, the large variation of breakpoints in capillary desaturation curves has for the first time been partially explained as resulting from the factor $k^r(S)P_\mathrm{c}(S)$ in eq. (27). *[11.1.0.6]* Finally, the article analyzes the plateau saturation and breakpoint in capillary desaturation curves. *[11.1.0.7]* Based on the traditional two-phase flow theory the breakpoint may vary by several decades. *[11.2.0.8]* It is found that this variation depends not only on capillary number but also on protocol, initial conditions, boundary conditions and other details of the capillary desaturation experiment.

¶Simple percolation models [49], while containing a diverging length scale at the pecolation transition, are difficult to apply in the present context, because of very strong geometric correlations and because invasion percolation models are limited to the slow drainage limit.

## Acknowledgments

Data presented in Figure 1 were collected at the Swiss Light Source, Paul Scherrer Institute, Villigen, Switzerland. One of us (R.H.) is grateful to Axel Makurat and Shell Global Solutions B.V. for their hospitality in Amsterdam and to the Deutsche Forschungsgemeinschaft (DFG) for financial support.

## References

[1] A. Abrams, Soc. Petr. Eng. Journal **15**, 437 (1975).
[2] N. Wardlaw and M. McKellar, The Canadian Journal of Chemical Engineering **63**, 525 (1985).
[3] L. Lake, *Enhanced Oil Recovery* (Prentice Hall, Englewood Cliffs, 1989).
[4] J. Melrose and C. Brandner, J.Can.Pet.Technol. **13**, 64 (1974).
[5] R. Armstrong, A.Georgiadis, H. Ott, D. Klemin, and S. Berg, Geophysical Research Letters **41**, 1 (2014a).
[6] R. Armstrong and S. Berg, Phys.Rev.E **88**, 043010 (2013).
[7] R. Armstrong, N. Evseev, D. Koroteev, and S. Berg, Advances in Water Resources **77**, 57 (2015).
[8] F. Dullien, *Porous Media - Fluid Transport and Pore Structure* (Academic Press, San Diego, 1992).
[9] R. Hilfer, Advances in Chemical Physics **XCII**, 299 (1996).
[10] R. Larson, H. Davis, and L. Scriven, Chemical Engineering Science **36**, 75 (1981).
[11] A. Georgiadis, S. Berg, A. Makurat, G. Maitland, and H. Ott, Phys.Rev.E **88**, 033002 (2013).
[12] A. Payatakes, Ann.Rev.Fluid Mech. **14**, 365 (1982).
[13] R. E. Hinkley, M. M. Dias, and A. C. Payatakes, PCH PhysicoChemical Hydrodynamics **8**, 185 (1987).
[14] R. Lenormand, Journal of physics C **2**, 79 (1990).
[15] R. Hilfer, Physical Review E **58**, 2090 (1998).
[16] R. Hilfer and H. Besserer, in *Porous Media: Physics, Models, Simulation*, edited by A. Dmitrievsky and M. Panfilov (World Scientific Publ. Co., Singapore, 2000) p. 133.
[17] R. Hilfer and H. Besserer, Physica B **279**, 125 (2000b).
[18] R. Hilfer, Physica A **359**, 119 (2006a).
[19] R. Hilfer, Phys.Rev.E **73**, 016307 (2006b).
[20] R. Hilfer, Physica A **371**, 209 (2006c).
[21] R. Hilfer, in *CP1091, Modeling and Simulation of Materials*, edited by P. Garrido, P. Hurtado, and J. Marro (American Institute of Physics, New York, 2009) p. 141.
[22] R. Hilfer and F. Doster, Transport in Porous Media **82**, 507 (2010).
[23] F. Doster, P. Zegeling, and R. Hilfer, Physical Review E **81**, 036307 (2010).
[24] F. Doster and R. Hilfer, New Journal of Physics **13**, 123030 (2011).
[25] F. Doster, O. Hönig, and R. Hilfer, Phys.Rev.E **86**, 016317 (2012).
[26] R. Hilfer, F. Doster, and P. Zegeling, Vadose Zone Journal **11**, vzj2012.0021 (2012).
[27] F. Doster and R. Hilfer, Water Resources Research **50**, 1 (2014).
[28] M. Reed and B. Simon, *Methods of Modern Mathematical Physics*, Vol. I: Functional Analysis (Academic Press, New York, 1972).

[29] R. Hilfer, in *Räumliche Statistik und Statistische Physik*, Vol. Lecture Notes in Physics, Vol. 554, edited by D. Stoyan and K. Mecke (Springer, Berlin, 2000) p. 203.

[30] R. Hilfer, Transport in Porous Media **46**, 373 (2002).

[31] V. Jikov, S. Kozlov, and O. Oleinik, *Homogenization of Differential Operators and Integral Functionals* (Springer, Berlin, 1994).

[32] R. Hilfer and P. Øren, Transport in Porous Media **22**, 53 (1996).

[33] E. Buckingham, *Studies on the movement of soil moisture*, Tech. Rep. (U.S.Department of Agriculture, Bureau of Soils, 1907).

[34] L. Richards, Physics **1**, 318 (1931).

[35] R. Wyckoff and H. Botset, Physics **7**, 325 (1936).

[36] M. Muskat and M. Meres, Physics **7**, 346 (1936).

[37] M. Leverett, Trans. AIME **142**, 152 (1941).

[38] D. Weitz, J. Stokes, R. Ball, and A. Kushnik, Phys. Rev. Lett. **59**, 2967 (1987).

[39] A. Calvo, I. Paterson, R. Chertcoff, M. Rosen, and J. Hulin, J. Coll. Interface Sci. **141**, 384 (1991).

[40] L. Anton and R. Hilfer, Physical Review E **59**, 6819 (1999).

[41] E. Ojeda, F. Preston, and J. Calhoun, Producers Monthly **18**, 20 (1953).

[42] F. Kalaydijan, Transport in Porous Media **5**, 215 (1990).

[43] R. Bentsen, Journal of Petroleum Science and Engineering **48**, 81 (2005).

[44] V. Joekar-Niasar, F. Doster, R. Armstrong, D. Wildenschild, and M. Celia, Water Resources Research **49**, 4244 (2013).

[45] M. Rücker, S. Berg, R. Armstrong, A. Georgiadis, H. Ott, A. Schwing, R. Neiteler, N. Brusse, A. Makurat, L. Leu, M. Wolf, F. Khan, F. Enzmann, and M. Kersten, Geophysical Research Letters, in press (2015).

[46] R. Armstrong, H. Ott, A. Georgiadis, M. Rücker, A. Schwing, and S. Berg, Water Resources Research **50**, 10.1002/2014WR015858 (2014b).

[47] W. Haines, The Journal of Agricultural Science **20**, 97 (1930).

[48] F. Moebius and D. Or, Journal of Colloid and Interface Science **377**, 406 (2012).

[49] D. Stauffer and A. Aharony, *Introduction to Percolation Theory* (Taylor and Francis, London, 1992).

[50] D. DiCarlo, J. Cidoncha, and C. Hickey, Geophysical Research Letters **30**, 1901 (2003).